BERYLLIUM-10 DERIVED EROSION RATES FROM THE HANGAY MOUNTAINS, MONGOLIA: LANDSCAPE EVOLUTION IN A PERIGLACIALLY-DOMINATED CONTINENTAL INTERIOR

A Thesis
Presented to
The Academic Faculty

by

Chelsea E. Hopkins

In Partial Fulfillment
of the Requirements for the Degree
Master's of Science in the
School of Earth and Atmospheric Science

Georgia Institute of Technology
December 2012

BERYLLIUM-10 DERIVED EROSION RATES FROM THE HANGAY MOUNTAINS, MONGOLIA: LANDSCAPE EVOLUTION IN A PERIGLACIALLY-DOMINATED CONTINENTAL INTERIOR

Approved by:

Dr. Judith Curry
for Kurt Frankel, Advisor (deceased)
School of Earth and Atmospheric Sciences
Georgia Institute of Technology

Dr. Karl Wegmann
School of Marine, Earth and Atmospheric Sciences
North Carolina State University

Dr. Andrew Newman
School of Earth and Atmospheric Sciences
Georgia Institute of Technology

Dr. Josef Dufek
School of Earth and Atmospheric Sciences
Georgia Institute of Technology

Date Approved: August 24, 2012

This thesis is dedicated to the memory of my adviser and friend, Dr. Kurt Frankel.

ACKNOWLEDGEMENTS

I wish to thank Dr. Kurt Frankel for sharing his knowledge and passion for geomorphology with me. His ability to make things such as a strath terrace the most exciting thing I learned in a week opened my eyes to the movements of the world around me like I had never known.

When Kurt passed away last summer, Dr. Karl Wegmann stepped in as my adviser and explained that he did still want my help two weeks later in Mongolia. I don't know if he knew how much work that would end up being as he pushed me all the way to the completion of this thesis, but I can't thank him enough for the support and smiles he always offered along the way.

Tina Marstellar provided daily assistance from teaching me everything in the lab, multiple times if necessary, to GIS tricks to reading my thesis to passing on knowledge from Kurt. I couldn't have done this without her knowledge and support and the fun we had along the way.

I would also like to thank Dr. Andy Newman for support he provided at Georgia Tech. Thanks to him and Dr. Joe Dufek, my thesis reading committee, for the helpful comments and suggestions to improve my thesis.

I wish to thank my parents, Chip and Anna Hopkins, for not letting me quit when I was ready to move back home. Their love and continual support mean more to me than they could ever know.

TABLE OF CONTENTS

LIST OF TABLES

LIST OF FIGURES

LIST OF ABBREVIATIONS

ELA	equilibrium line altitude
^{10}Be	beryllium-10
PRIME	Purdue Rare Isotope Measurement laboratory
HCl	hydrochloric acid
HF	hydrofluoric acid
HNO_3	nitric acid
AMS	accelerator mass spectrometer
DEM	digital elevation model
HI	hypsometric integral

SUMMARY

Terrestrial cosmogenic nuclides such as beryllium-10 have recently been used as a way to determine basin-average erosion rates around the world. These erosion rates are useful to geomorphologists investigating landscape evolution. The Hangay Mountains in Mongolia are a prime location to use beryllium-10 because of the granitic rocks that provide the quartz needed for cosmogenic analysis as well as the lack of observed evidence of recent or old mass wasting events that mobilize sediment and bedrock with much lower cosmogenic concentrations that cause underestimations of erosion rates.

Basin-average erosion rates observed in seven basins across the eastern Hangay Mountains range from 12 m/My to about 20 m/My. These are of similar magnitude to those found in tectonically inactive regions such as the southern Appalachians. Comparing basin-average erosion rates to basin parameters, whole basin relief had the highest calculated R^2 value and elevation had the lowest P-value. No strong relationships were seen between erosion rate and mean slope angle, hypsometric integral, area, or mean local relief.

The basin-average erosion rates observed in the Hangay were compared to previous studies by Ahnert (1970), Portenga and Biernman (2011), and Matmon et al. (2009). We found erosion rates from the Hangay to be much lower than expected in our analyses. The differences in erosion rates from the Hangay Mountains compared to other places around the world are likely due to the fact that the streams in the Hangay are eroding into alluvium as opposed to bedrock, and are located in a landscape dominanted by diffusive hillslope sediment transport mechanisms. The erosion rate is limited to the amount of sediment that can be transported by the streams.

CHAPTER 1

INTRODUCTION

Landscape Evolution Models

Within the field of geomorphology, the lifecycle of a mountain range is an important concept. Since the 1800's, geologist have tried to qualitatively explain the development, growth, and decay of mountain ranges. Influenced by the Great Unconformity of the Grand Canyon, John Powell (1875) first recognized the enormous effect erosion has on mountain ranges, namely, the ability to erode high relief areas to horizontal surfaces toward an elevation considered the "base level." William Davis (1889; 1899) built on Powell's idea to describe "The Geographic Cycle" which has four major stages. The first stage of the landscape is developed by rapid uplift and characterized by high mean elevation and low relief. The landscape develops into its second stage of youthful appearance when streams have irregular grades and have carved deep valleys. During this period, there is high mean elevation and high relief. Once the base level of elevation is reached by the streams in the valleys, "maturity", the third stage, of the landscape occurs when the rivers are graded and begin to erode laterally and the hillslopes begin to erode mostly by creep into more rounded forms. The last stage or "old age" phase of the mountain's lifecycle is reached when mean elevation and relief keep decreasing. The streams meander and create large flat floodplains in which the sediment can eventually only erode by hillslope creep. The end of the mountain's life cycle is this flat surface considered the penultimate plain or the "peneplain" (Pazzaglia, 2003).

In 1953, Walter Penck proposed an opposing theory of landscape development in which deformation increases to a maximum allowing for gradual topographic uplift and then the deformation rate slowly decreases back to zero where uplift would cease (Penck, 1953). According to Penck, erosion counteracted the building of topography throughout this process and after uplift concluded, erosion would dominate to gradually lower the topographic relief.

A third view of landscape evolution came in 1960, when J.T. Hack proposed his principle of dynamic equilibrium of a drainage system. In this model, all areas in a drainage system adjust relative to each other and erode at the same rate. Instead of eroding to a regional base level, the topography is defined by the resistance to erosion of rocks of differing lithologies. He explained his hypothesis by using the example of a slope being in equilibrium if material being eroded from its summit was equal to the material being eroded at its base. In Hack's view, relief must be higher in areas experiencing quicker uplift because more potential energy is needed to drive erosion down the hillsides. The topography of an area in dynamic equilibrium will be constant as long as its driving forces (tectonic uplift and isostacy) and resisting forces (erosion) remain balanced through time and the exposed geology remains the same.

The three basic landscape evolution theories differ in the duration and rate of tectonic forcing. Davis assumed instant, rapid uplift. Penck allowed uplift to increase and then slow down gradually. Hack used a constant uplift rate throughout his model. Kooi and Beaumont (1996) developed a surface-process model that brought all three models together by integrating channel incision, sediment transport, and hillslope erosion to allow the response of a landscape to depend on the type of tectonic forcing applied (Burbank & Anderson, 2012). Their numerical models predicts the lag time of the

landscape's response to the tectonic forcing. Although this model is highly simplified, it brings together all three of the older theories and shows they can all play a role in the evolution of a landscape.

Recent Studies

In 1970, Frank Ahnert published one of the first studies that compared erosion rates of twenty large, mid-latitude, temperate river basins to their mean local relief. He determined that basin-average erosion rates are linearly proportional to mean local relief. He proposed that to reduce the relief of a landscape to ten percent of its original relief would take 11 My. Including the influence of isostatic compensation, it would take a minimum of 18.5 My. In Ahnert's theory, Hack's dynamic equilibrium could only be achieved in the unlikely event that the rate of uplift was constant for at least 20 My.

The Hangay Mountains cover an area of ~200,000 km^2 in central Mongolia. Within this mountain range there are many high-elevation, flat-summit plateaus that span a few kilometers by tens of kilometers in size. These have previously been described as Mesozoic and early Cenozoic aged peneplains which have been preserved, and more recently uplifted by renewed vertical tectonic forces. Regions of these peneplains were uplifted during the late Cenozoic, creating the high elevation flat surfaces seen there today (Devyatkin, 1975; Cunningham, 2001; Jolivet et al., 2007). Slowly eroding summit surfaces characterize this hypothesis, while lower elevations experience faster erosion rates that have removed the remnants of the paleoerosion surface.

More recently, global and regional studies have shown that glacial and periglacial erosion can also affect the topographic evolution of a mountain range. Glaciers can limit the height a mountain range can achieve above the snowline, or glacier equilibrium line altitude (ELA; Egholm et al., 2009; Brozović et al., 1997)). This is evidenced by the bulk of the surface area occurring around the same elevation as the ELA, and that the heights

of the summits are usually within 1500m above the ELA (Egholm et al., 2009). Brozovic et al. (1997) explained the erosion above the ELA with two negative feedback mechanisms. First, if the ELA drops for reasons such as isostatic or tectonic uplift or climate related changes, the area of the glacier will cover more of the landscape and will allow more erosion to occur bringing the concentration of surface area back below the ELA. Secondly, if small peaks protrude above the glaciated landscape, they will attract moisture which speeds the erosional process to return the peak to a lower altitude. Hales and Roering (2009) suggest that frost-driven weathering processes can limit the surface relief at the ELA and could also limit the height of mountain summits.

Terrestrial Cosmogenic Nuclides

Previous Studies

Since the mid 1980's, beryllium-10 (^{10}Be) has been effectively used in many geomorphic studies including channel sediment dynamics (Belmont et al., 2007), river incision rates and formation of fluvial terraces (Burbank et al., 1996; Hancock et al., 1998; Cyr and Granger, 2008; Fuller et al.,2009), glacial moraines (Finkel et al., 2003), cave sediments (Refsnider, 2010), summit erosion rates and relief production measurements (Hancock and Kirwan, 2007; Small et al., 1997), fault offset landforms (Frankel et al., 2010), and catchment-averaged erosion rates (Granger et al., 1996; Matmon et al., 2003; von Blackenburg, 2005; Stock et al., 2009; Cyr et al., 2010).

In the Gobi-Altay range of Mongolia, Vassallo et al. (2011) used ^{10}Be to look at the exposure histories of individual clasts and how geomorphic processes can affect the cosmogenic signals. They looked at samples from sites before and after the depositional process, and concluded that knowledge of the pre- and post-depositional processes will allow for a more nuanced understanding in the analysis and interpretation of ^{10}Be results.

Cosmogenic Nuclide Theory

Terrestrial cosmogenic nuclide geochronology can be utilized to find erosion rates of a surface as well as the average erosion rate of an entire drainage basin. Cosmic radiation interacts with minerals in rocks to supply a quantifiable history of the rock's exposure near the Earth's surface (Gosse and Phillips, 2001). The cosmogenic nuclide ^{10}Be is produced by a combination of spallation and muonic components. High-energy nucleons (protons and neutrons), cosmic radiation generated mostly from within our galaxy, make their way through the earth's magnetic field and react with particles in the atmosphere (Gosse and Phillips, 2001). These reactions produce secondary radiation composed of secondary nucleons and mesons that have the same characteristics as primary radiation. Because there is a greater density of these high-energy particles after the first reactions, many more reactions become possible in the atmosphere and continue into the rock at the earth's surface. This is known as the cosmic-ray cascade (Figure 1).

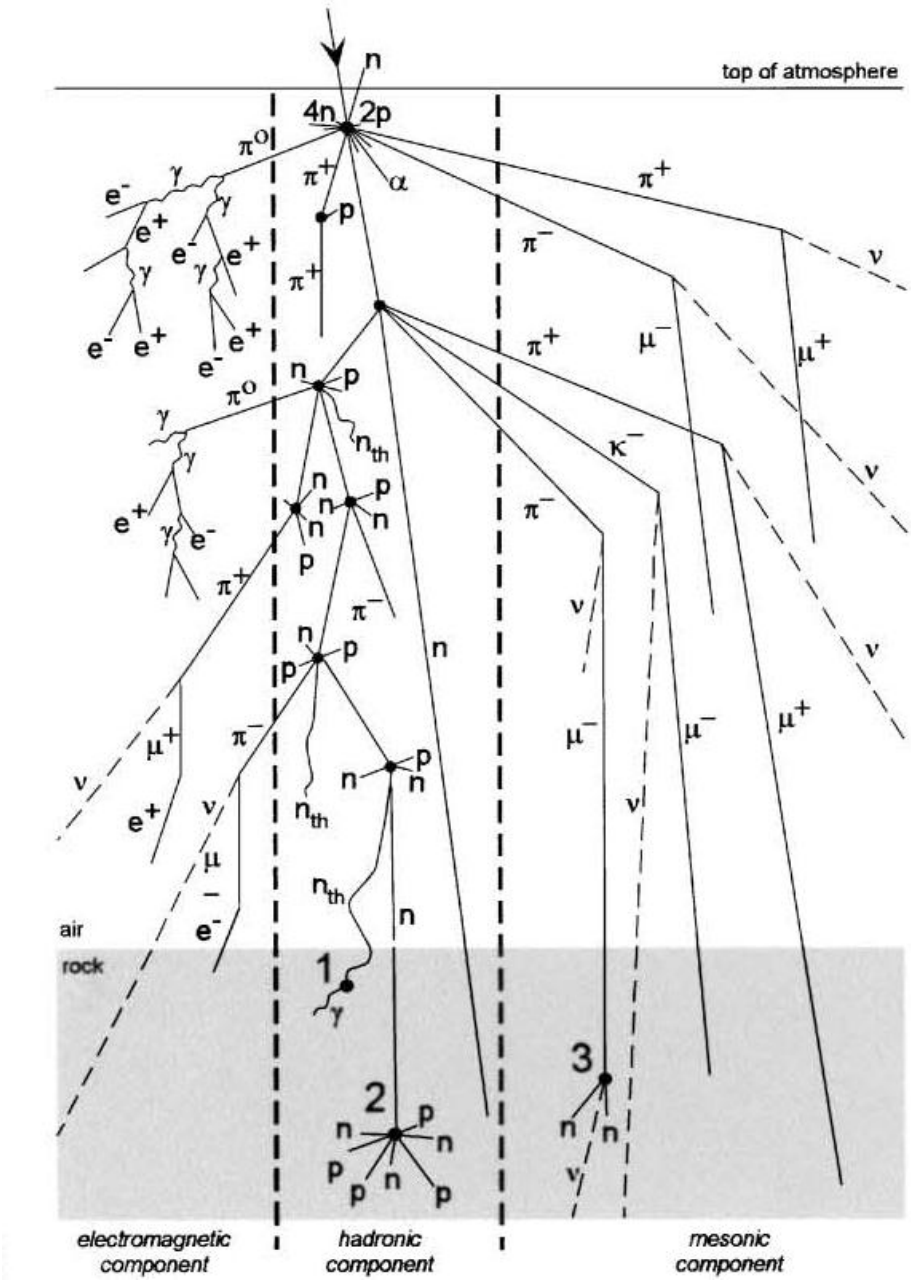

Figure 1. A cosmic ray particle as it enters the atmosphere and begins the cosmic-ray cascade. From Gosse and Phillips (2001).

Because the primary targets for spallation are oxygen and silicon, quartz is an ideal target mineral. Its abundance in crustal rocks, simple composition, and ease of separation from other minerals are additional reasons that using quartz in ^{10}Be analysis is ideal (Bierman et al., 2002).

Once the atomic collisions begin in rock at the earth's surface, the particles quickly lose energy and cosmogenic nuclide production declines as a function of depth,

$$P(z) = P_0 e^{-(\frac{z\rho}{\Lambda})} \quad (1)$$

where z is depth, P_0 is the surface production rate [atoms g^{-1} yr^{-1}], ρ is the material's density [g cm^{-3}], and Λ is the mean attenuation depth [g cm^{-2}] (Bierman and Steig, 1996). For ^{10}Be, cosmogenic nuclide production becomes negligible around an attenuation depth of 60 cm in rock, allowing a baseline concentration to be determined, if necessary (Balco et al., 2008). This baseline concentration can be used to identify pre-depositional history known as inheritance and can be useful in other geomorphic studies such as depositional river terraces as shown in Anderson et al. (1996).

Beryllium-10 is also produced in the atmosphere as a meteoric cosmogenic nuclide. This atmospheric component can be up to 10^3 greater than the rate at which ^{10}Be is produced in rocks (Gosse and Phillips, 2001). The atmospheric component must be removed from the terrestrially produced ^{10}Be in the laboratory in order to obtain relevant terrestrial nuclide concentrations. This atmospheric component can easily be removed when working with quartz (lab methods discussed in Chapter 2).

Production rates have been reported for high latitude (defined as 60° and above) and sea level from 4.5 to 6.4 atoms g^{-1} yr^{-1} (Gosse and Phillips, 2001). There is still much debate as to how these production rates vary with time and the best way to incorporate these variations into the age calculations has yet to be determined (e.g. Lal, 1991; Stone, 2000; Dunai, 2000; Desilets and Zreda, 2003; Lifton et al., 2005; Desilets et al., 2006; Balco et al., 2008). Because a consensus has not been reached on the best method to model time-variable production rates, we chose to use the time-invariant model. A sea level, high latitude value of 5.13 atoms g^{-1} yr^{-1} based on Lal (1991) was used in this study to determine erosion rates. There are three major corrections that should be made: latitude and altitude correction (Lal, 1991; Stone, 2000) along with a correction for local topographic shielding (Gosse and Phillips, 2001). The intensity of cosmic rays increase as

atmospheric pressure decreases; therefore higher altitudes and latitudes will experience higher production rates (Stone, 1999). Also, modifications will need to be used to scale in-situ ^{10}Be production to a corrected site specific value because production rate is affected by the geomagnetic field of the earth (Gosse and Phillips, 2001), the intensity of which changes with latitude and altitude. Lastly, the standard production rate model assumes horizontal surfaces for its calculations. Localized topographic shielding can decrease the amount of cosmic rays reaching the surface and consequently decrease the local site-specific production rate (Gosse and Phillips, 2001).

By measuring the concentration of ^{10}Be in a certain amount of quartz, the exposure time can be determined from the following equations

$$C_{total} = \frac{P_B e^{-(\frac{z\rho}{\Lambda})}}{\lambda'}\left(1 - e^{-\lambda' T}\right) + C_{initial} \quad (2)$$

$$\text{and} \quad \lambda' = \lambda\left(1 + \frac{\varepsilon\rho}{\lambda\Lambda}\right) \quad (3)$$

where C is concentration [atoms g^{-1}], T is exposure time [yr], λ is the decay constant [yr^{-1}], and ε is the erosion rate [cm yr^{-1}]. For locations that have been exposed for longer than the mean life of ^{10}Be, the erosion rate can be determined by

$$\varepsilon = \frac{P_0 \Lambda}{C\rho} \quad (4)$$

from Granger et al. (1996). The concentration of ^{10}Be is found by taking a sufficient amount of sample from the field location, passing it through a series of mechanical and chemical procedures to get pure quartz, extracting beryllium from the quartz, and measuring the amount of beryllium using an accelerator mass spectrometer.

Erosion Rate Determination

By finding the concentration of the nuclide ^{10}Be, a history of how long rock material has been near the surface of the Earth can be determined. High concentrations of ^{10}Be atoms correspond to a slow erosion rate because the rock has been exposed to the surface for an extended amount of time allowing a build up to ^{10}Be atoms. On the other

hand, low concentrations of ^{10}Be atoms would imply faster erosion rates because the rock has been eroded from the surface before a larger amount of ^{10}Be atoms could accumulate. One can get a bedrock erosion rate by taking a sample from an exposed rock on a hillslope and determining the concentration of ^{10}Be atoms within it. A slow erosion rate would correspond to a very old age. Eventually radionuclides like ^{10}Be reach a point where the rate at which ^{10}Be is being produced equals the rate of its decay. This is called secular equilibrium and occurs around 4 My for ^{10}Be (Walker, 2005). Therefore, the existence of a peneplain would also be supported by ages near secular equilibrium.

Secondly, a rate of erosion can be found for the sediment transported through an entire drainage basin (Granger et al., 1996). In this case, all the bedrock along the hillslopes will erode at its own pace and be transported and mixed down the hillsides and through the drainage network. Each sediment grain will hold a nuclide concentration the same as the bedrock it was eroded from. By taking an aggregated sample from an active river channel, the erosion rates for all points on the hillsides draining into an outlet spot will be averaged. The end result is a basin averaged erosion rate. By comparing the ridgeline (bedrock) and the basin averaged erosion rates, one can determined how and if relief is changing.

Research Goals

This study includes seven basin-average samples taken from the Hangay Mountains, Mongolia. Erosion rates determined from these samples can give us insight into how the Hangay Mountains fit into the different landscape evolution models. Erosion rates are compared to basin parameters such as latitude, elevation, relief, mean slope, hypsometric integral, etc. to investigate statistical relationships.

The basin-average erosion rates determined in the Hangay Mountains will be compared to the Ahnert (1970) dataset, the Portenga and Bierman (2011) world-wide

compilation of basin-average erosion rates, and a study by Matmon et al. (2009) to assess how the erosion rates from this periglacial setting in the Hangay Mountains compare to others from environments around the world. Also, Landman (2007) studied apatite grains in the same study area to determine the cooling ages of late Paleozoic and early Mesozoic granites. These ages are used to determine an example of how the beryllium-10 derived erosion rates compare to a possible long-term exhumation rate of the Hangay.

CHAPTER 2

METHODS

Field Sampling

Samples from the study area were collected to determine catchment averaged erosion rates. Samples were taken of fluvial sand from active stream beds or sand bars within the stream channel and were chosen based on ease of access, size of the drainage basin, and rock type (Figure 2). Figure 3 shows the locations of the samples with their corresponding drainage areas.

Figure 2. Example of a catchment-averaged sample site.

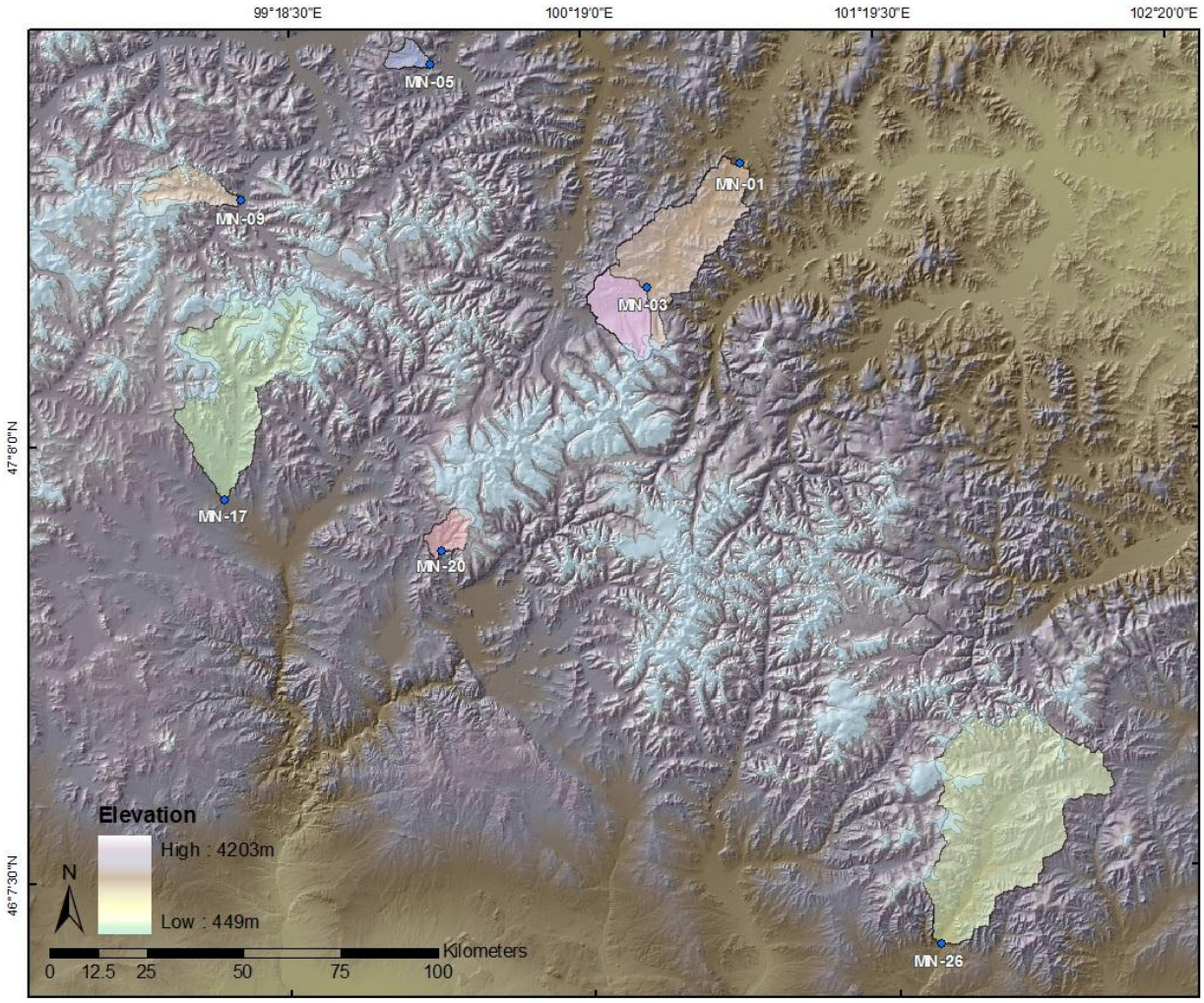

Figure 3. Digital elevation model of the Hangay Mountains with basin sample locations shown as blue dots. Shaded regions associated with the basin samples show the up-basin area draining into the sampling location. Light blue shade shows ELA area of 2600 m.

An averaged erosion rate can be found for the upstream catchment area draining to a point by taking an aggregated sample (von Blackenburg, 2005). This method is based upon the assumption that, although all areas in a catchment may erode at different rates, the eroded sediment is mixed as it is transported downstream to a common outlet spot. As such each component of the landscape will contribute an amount of sediment at the sampling site proportional to its erosion rate based on equation (4). This is schematically

shown in Figure 4 using a simulated basin where each pixel contributes its specific erosion rate to the sediment at the outlet of the catchment (Gosse, 2009).

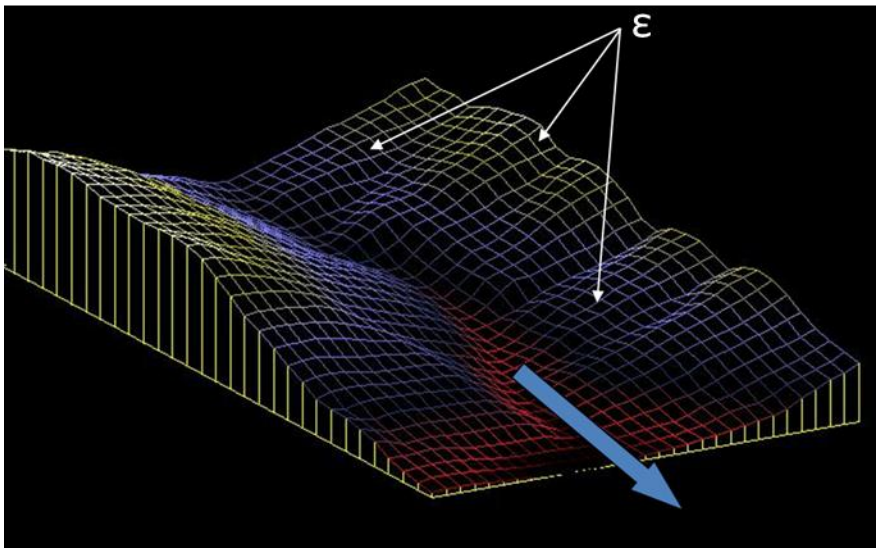

Figure 4. Simulated basin where each pixel contributes a particular erosion rate (shown by colors), ε, per equation (4) to the sediment at the outlet of the entire basin therefore allowing the erosion rate at the outlet to be considered as catchment averaged. From Gosse (2009).

Von Blackenburg (2005) also laid out the assumptions made when using the concept of basin-averaged erosion, which include uniform denudation throughout the catchment, that every region must supply part of the sample proportional to its erosion rate, that eroded grain size distribution must be nearly the same for different rock types, and that the time scale for denudation is shorter than the radioactive decay for the isotope's time scale. Matmon et al. (2003) demonstrated the feasibility of basin-averaged erosion from the Great Smoky Mountains of the southern Appalachians, by taking samples from tributaries and the main channels of two catchments along with a sample from the confluence of the two main channels. The erosion rates found from the tributaries are averaged at points downstream of those tributaries on the main channels. At the confluence between the two tributaries, the basin average erosion rate was found to be the mean of the separate sub-basins. (Figure 5; Matmon et al., 2003). This also

suggests that sediment storage within the basin is negligible compared to the accumulation of cosmic rays in altering the average erosion rate.

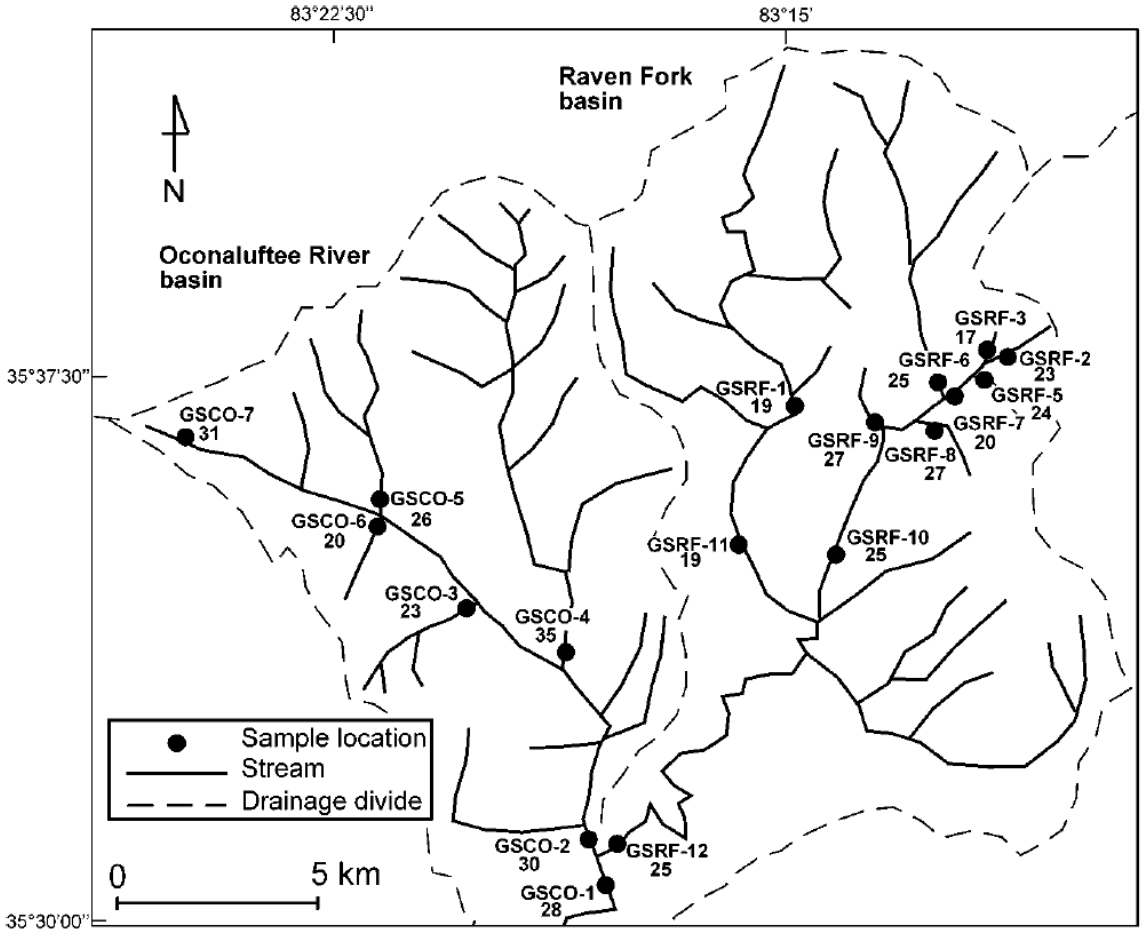

Figure 5. Basin in the Great Smoky Mountains. Erosion rates are shown in numbers below sample names. Catchment erosion rate averaging can been seen downstream of tributaries and between Oconaluftee River and Raven Fork basins. From Matmon et. al, 2003.

Laboratory Processing

Once the sample is collected from the field and returned to the laboratory, the beryllium must be separated to find the concentration for erosion rate calculations. Initially, the field sample would need to be physically processed by crushing ridge top samples 250 micron to 500 micron grain size. To be consistent, the catchment-averaged samples are sieved and the 250 micron to 500 micron grain sizes are used. Because of

lack of material in this size range, 250 micron to 750 micron grain sizes were used for the catchment-averaged samples .Within this grain size range, direct comparisons can be made between erosion rate and the eroding process. To first begin physically purifying the sample to quartz, a Frantz magnetic separator was utilized. This process separates magnetic from nonmagnetic grains. Since quartz is not magnetic, just the nonmagnetic portion is used for the chemical process.

The process currently used at Georgia Institute of Technology's Frankel Terrestrial Cosmogenic Nuclide Geochronology Lab was modified from Bierman et al. (2002; see Appendix A). After the correct grain size is acquired and magnetic separation has been performed, the chemical process to get from sediment and crushed rock to pure quartz can begin. The first step is a hydrochloric acid (HCl) leach which dissolves and removes the carbonates, iron oxides, and organic materials from the sample. After this is complete and the sample is dried and weighed, a series of three ultrasonic leaches in a mixture of hydrofluoric acid (HF) and nitric acid (HNO_3) are performed to isolate the pure quartz and remove the atmospheric ^{10}Be-derived component. Between each leach, the sample was dried and weighed. Once these are completed, the sample is pure quartz. If not, the process is repeated until the sample is sufficiently pure quartz. The amount of pure quartz needed for accelerator mass spectrometer measurements is a function of the sample's location and estimated age. The amount can be determined by using the quartz calculators found at http://shadow.eas.gatech.edu/~kfrankel/facilities.htm. For this sample location, about 70 g of quartz was determined to be sufficient to get a ^{10}Be concentration.

After the quartz purification steps have been completed and the amount of quartz is determined, a known amount of ^{9}Be carrier is added and the quartz is heated and dissolved into solution with HF. The solution is dried down. Any trace amounts of fluorides are converted to perchlorates by a sequence of three perchloric fuming steps.

For each group of samples in the beryllium isolation stages, a laboratory blank is also run with only the ^{9}Be carrier added. This blank will allow the amount of ^{10}Be and ^{9}Be from the laboratory atmosphere to be measured.

Next, the sample goes through ion exchange chromatography using anion and cation columns. These steps isolate the beryllium from the sample. The beryllium is then dried down and ignited at 750°C to convert beryllium hydroxides to beryllium oxides. The beryllium can then be packed into an accelerator mass spectrometer (AMS) cathode using niobium and sent to the AMS at Purdue University's Rare Isotope Measurement laboratory (PRIME) for analysis.

Laboratory Results to Erosion Rates

The accelerator mass spectrometer analysis measures the ^{10}Be/^{9}Be ratio and a one standard error uncertainty for each sample. Following the process outlined by Balco (2006), the ^{10}Be/^{9}Be ratio is used to determine a sample ^{10}Be concentration. The mass of the ^{9}Be carrier added, the average number of ^{10}Be atoms in a blank for a particular laboratory run, and their uncertainties, as well as the mass of quartz used in the sample are all needed quantities. Assuming that the amount of ^{9}Be from the lab atmosphere is much less than the ^{9}Be carrier added and that the number of ^{10}Be atoms added with the carrier is the same in the blank as in each sample, the ^{10}Be/^{9}Be ratio can be determined as

$$^{10/9}Be = \frac{N_{10}M_q + n_{10,B}}{n_{9,C}} \quad (5)$$

where N_{10} is the concentration of ^{10}Be [atoms g^{-1}], M_q is the mass of quartz in the sample [g], and small *n* represents the number of atoms with subscripts 9 or 10 for the type of beryllium, and B or C for blank or carrier, respectively. The number of atoms of ^{10}Be in the carrier is determined by the molar weight of beryllium and the mass of the added carrier. To get the concentration of ^{10}Be from each sample, the equation is solved for N_{10}:

$$N_{10} = \frac{1}{M_q}\left(\frac{^{10/9}Be M_C N_A}{A_{Be}} - n_{10,B}\right) \quad (6)$$

where M_C is the mass of Be in the carrier [g], N_A is Avogadro's number [6.022x10^{23} atoms mol^{-1}], and A_{Be} is the molar weight of Be [9.012 g mol^{-1}].

Sources of uncertainty in the concentration are in the isotope ratio measurement (given with the accelerator mass spectrometer results), the number of atoms in the blank, and the mass of Be added in the carrier (Balco, 2006). The equation for uncertainty can be found by adding the sources of error in quadrature.

With the concentration of ^{10}Be (N_{10}) and the error associated with that number (error N_{10}), one now needs to determine a site specific production rate to use in calculating the erosion rate for each sample. This can be done by following the process detailed in Balco (2001). A digital elevation model (DEM) of the field area should be obtained. The higher the resolution of the DEM, the longer the computational time needed to calculate each step. So, the resolution must be taken into account when processing a DEM. A DEM with 160 m resolution was used for this report's calculation of production rates. For each basin-wide sample, the area that drains into the location the sample was taken must be determined. This can be done using the *flowdirection* and *flowaccumulation* routines in ArcGIS. As mentioned before, a baseline production rate is scaled by a latitude/altitude correction and a topographic shielding factor. Both are calculated for each pixel in the catchment's area, and then summed as a total correction for each pixel in MATLAB. This total correction matrix is multiplied by the baseline production rate to achieve a unique production rate for each pixel. These are then averaged to find a production rate for the entire catchment. The Cosmocalc extension for Excel (Vermeesch, 2007) can be used with scaling factors found from the total correction matrix to get erosion rates from each of five different scaling models – Lal (1991), Stone (2000), Dunai (2000), Desilets and Zreda (2003), and Desilets et al. (2006).

Computing Basin Parameters

Erosion rates are compared to multiple parameters of the basins to see if any statistical relationships emerge. Latitude and elevation are both taken from the sampling location. Whole basin relief is calculated as the difference in the highest and lowest elevations in the basin. For basins with areas greater than 50 km^2, mean basin relief is determined. Relief is calculated for each of the tributary drainage areas and averaged to find mean basin relief. Hypsometric integral, HI, is defined by the equation:

$$HI = \frac{z_{mean} - z_{min}}{z_{max} - z_{min}} \tag{7}$$

where z is the elevation. Mean slope is found using by averaging the slope of each pixel throughout the basin. The width of the valley floor immediately above the sampling location (5 km) was calculated at one-kilometer spacing in Google Earth to find the average valley width.

CHAPTER 3

STUDY AREA: HANGAY MOUNTAINS, MONGOLIA

Tectonic Setting

The Hangay Mountains or Dome is a ~200,000 km^2 uplift embedded within the larger Mongolian Plateau (~425,000km^2; Figure 6). Thrust faults accommodate far-field compression from the India-Asia collision to the south of the Hangay and transition into extensional deformation north of the Hangay shown in the Hovsgol and Baikal Rifts. The Hangay Dome is contained by active strike slip faults to the North (Bulnay fault system), South (Gobi Altai fault system), and West (Mongolian Altai fault system). Minor extensional faulting characterizes the area within the dome (Walker et. al, 2007).

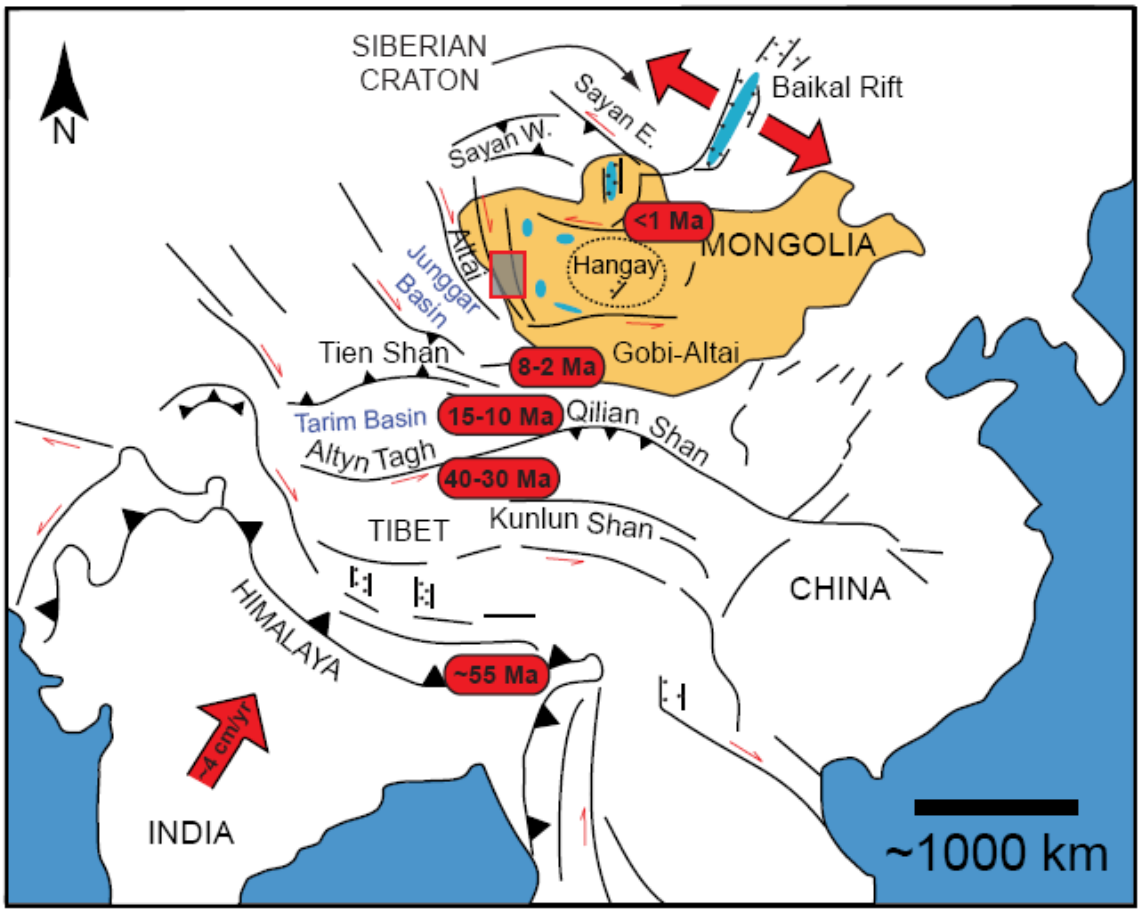

Figure 6. Tectonic setting of the Hangay Dome showing the far field India-Asia collision, modified from Vassallo et al. (2007).

Geomorphology

The dome itself sits about 1.5 km above the surrounding plateau region and reaches elevations of 4000 m. The Hangay Mountains are characterized by high elevation, low relief surfaces that have previously been assumed to be the remnants of a Mesozoic to early Cenozoic aged regional erosional surface (peneplain) that has been recently uplifted during the late Cenozoic (Devyatkin, 1975; Cunningham, 2001; Jolivet et al., 2007). These high elevation, flat surfaces create a main drainage divide that separates waters draining northward into the Selenga River, a tributary to Lake Baikal and eventually Arctic Ocean, from waters draining south and west into the internall-drained Valley of Lakes and Mongolian Depression of Lakes, respectively (Figure 6).

The landscape of the Hangay Mountains is dominated by upwardly convex hillslopes which suggest that the active sediment transport processes are diffusional (Figure 7, e.g. Gilbert, 1909). Frost cracking and frost shattering occur when water gets in existing cracks and joints and expands as it freezes. This deepens the joints and can eventually lead to breakdown of the rock creating scree which is then moved down slope by gravitational dominated transport (Hales and Roering, 2009).

This landscape is also devoid of large mass-wasting events such as landslides and rock avalanches making the locale more desirable for the use of cosmogenic nuclides in determining catchment wide erosion rates. Because the concentration of the nuclide is dependent on the time the material is exposed at or near the surface, a deep-seated landslide would expose and transport material with much lower concentrations than the surrounding areas. This newly uncovered material would decrease the average concentration for the whole basin; therefore, erosion rates would be underestimated (Niemi et al., 2005). Although, this material could provide useful information in areas with many landslides, variability caused by the mixing of less exposed material is still being explored and quantified (Yanites et al., 2009).

Figure 7. Two examples of convex-up hillslopes suggesting diffusional erosion thoughout the Hangay Mountains.

In the highest elevations of the Hangay Mountains, there are many signs of Quaternary glaciation. Field evidence includes erosional landforms such as cirques, tors, and U-shaped valleys, and depositional landforms like moraines (Figure 8). Regions that are thought to have been glaciated during the Last Glacial Maximum (LGM) are based on field observations and a mean ELA of 2600 m (Lehmkuhl et al., 2004).

Figure 8. Glacial landforms such as U-shaped valleys and moraine-dammed lakes (A, D), tors (B), and cirques (C) can be found in the high elevations of the Hangay Mountains.

Sample Sites

Seven ridgetop samples were taken from the eastern part of the Hangay. All samples with their locations and elevation are shown in Table 1. The sample locations as well as the last glacial maximum ELA area are shown on the map in Figure 3.

Table 1. Samples with location, elevation, and rock type.

Sample	Latitude (N)	Longitude (E)	Elevation (m)	Rock Type
MN-01	47.7777	100.8580	1813	granitic
MN-03	47.4960	100.5299	1995	granitic
MN-05	48.0186	99.7980	2110	granitic
MN-09	47.7086	99.1440	2275	metasediment/granitic
MN-17	47.0142	99.0879	2064	metasediment
MN-20	46.8927	99.8209	2200	granitic
MN-26	45.9615	101.4662	1809	granitic

Overall, the surface geology of the Hangay Mountains is dominated by granitic rocks. All of the samples except sample MN-09 were dominated by one rock type, either granites or metasedimentary rocks. The active stream channel from which sample MN-09 was taken contained a mix of granitic and metasedimentary rocks. Because there is a possibility of more quartz in the granites, this mixture of sediments could alter the calculated basin-average erosion rate because it would not satisfy the assumption that every region within the drainage basin must supply part of the sample proportional to its erosion rate (von Blackenburg, 2005). If the areas in the drainage basin dominated by metasedimentary rocks supplied less quartz to the active stream channel than the surrounding granitic areas, the erosion rate would be biased towards the erosion rates of the granitic areas.

CHAPTER 4

RESULTS

Erosion Rates

The basin-average erosion rates were calculated using CosmoCalc (Vermeesch, 2007) for five different production rate models (Lal,1991; Stone, 2000; Dunai, 2000; Desilets and Zreda, 2003; Desilets et al., 2006). Table 2 shows the results found from each of these models. All of the production rate models result in very similar erosion rates. From these, I have chosen Lal's model (1991) with a production rate of 5.13 atoms g^{-1} yr^{-1} for use in the following analysis and discussion, and the derived erosion rates shown next to their appropriate basin are in Figure 9. Erosion rates vary from about 12 m/My to just over 20 m/My.

Table 2. Erosion rates and associated 1-standard error found from CosmoCalc (Vermeesch, 2007). Note: Lal (1991) results are used for following discussions.

	Lal,1991		Stone, 2000		Dunai, 2000		Desilets & Zreda, 2003		Desilets et al. 2006	
Sample Name	Erosion rate (m/My)	Error (1σ)	Erosion rate (m/My)	Error (1σ)	Erosion rate (m/My)	Error (1σ)	Erosion rate (m/My)	Error (1σ)	Erosion rate (m/My)	Error (1σ)
MN-01	16.45	0.39	16.67	0.39	16.50	0.39	15.90	0.37	16.38	0.39
MN-03	20.14	0.85	20.41	0.86	20.20	0.85	19.46	0.82	20.04	0.85
MN-05	12.26	0.77	12.42	0.78	12.29	0.77	11.84	0.74	12.20	0.76
MN-09	12.51	0.83	12.68	0.84	12.55	0.83	12.08	0.80	12.45	0.82
MN-17	19.56	0.40	19.82	0.41	19.62	0.41	18.90	0.39	19.47	0.40
MN-20	16.58	0.96	16.80	0.97	16.63	0.96	16.02	0.93	16.50	0.95
MN-26	17.68	0.43	17.91	0.44	17.73	0.44	17.08	0.42	17.59	0.43

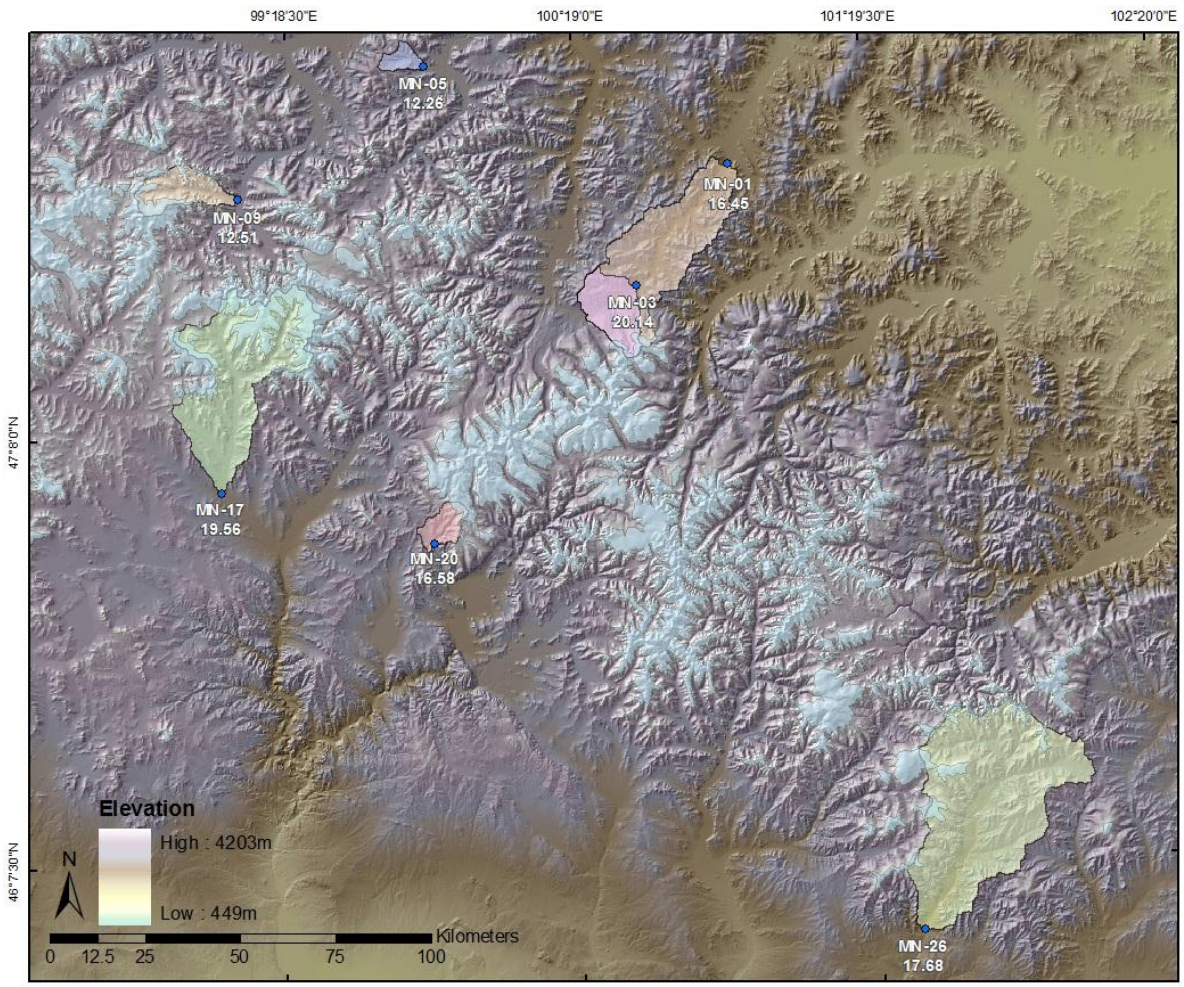

Figure 9. Digital elevation model of the Hangay Mountains. Blue dots show sample locations with corresponding drainage area shown by colored polygons. Erosion rates indicated beneath sample name are in m/My. The last glacial maximum ELA is shown shaded in as light blue.

Basin Parameters

Sample location elevations ranged from around 1800 m to almost 2300 m. Basin relief ranged from 617 m found in Basin 3 to 1371 m in Basin 1. Mean local relief was found in basins with areas larger than 50km^2 (basins 1, 17, and 26) by averaging relief of the main tributary drainage basins. These decreased the range in mean local relief to between 617 and 1195 m. The hypsometric integrals of individual basins vary from 0.28 to 0.44. The mean slope steepness by basin varies from 8.2° to 13.6°. The absolute value of the mean sine of the slopes varies from 0.37 to 0.98. Basins were chosen over a range

of areas from small tributaries of about 6 km^2, to large streams with a drainage area of nearly 1700 km^2. The width of the valley floor immediately above the sampling location (5 km) was calculated at one-kilometer spacing in order to see if valley width, as a proxy for floodplain storage of sediment, might be impacting the calculated basin-average erosion rates. Average valley floor widths ranged from 123 to 1943 m. Table 3 provides all basin parameters with erosion rates.

Table 3. Basin parameters.

Sample Name	Latitude (N)[a]	Elevation (m)[b]	Whole Basin Relief (m)	Mean Local Relief (m)	Hypsometric Interval	Mean Basin Slope (°)	Basin Area (km^2)	Valley Width (m)	Erosion rate (m/Mr)	Error (1σ)
MN-01	47.7777	1813	1371	667*	0.28	8.2	916.81	1178.31	16.45	0.39
MN-03	47.4960	1995	1195	1195	0.31	8.5	24.63	1428.98	20.14	0.85
MN-05	48.0186	2110	617	617	0.39	8.5	5.77	478.32	12.26	0.77
MN-09	47.7086	2275	1049	1049	0.40	13.6	20.85	695.61	12.51	0.83
MN-17	47.0142	2064	1282	752*	0.44	10.8	1028.99	1943.49	19.56	0.40
MN-20	46.8927	2200	883	883	0.36	8.4	9.94	122.61	16.58	0.96
MN-26	45.9615	1809	1339	823*	0.44	9.8	1653.53	600.11	17.68	0.43

[a]Latitude at sampling location.

[b]Elevation at sampling location.

*For basins with an area larger than 50km^2, mean local relief was calculated by averaging parameters of the tributaries

Erosion rates were compared to each of these basin parameters to investigate statistical relationships. Plots of erosion rate versus each basin parameter are shown in Figure 10. The P-values and R^2-values for each comparison are shown in Table 4. The R^2-value or coefficient of determination describes how much of the variance of a dataset is represented by the linear regression. The P-value explains the probability that an observed result could occur randomly. Therefore, a high P-value proposes that a dataset is random compared to another dataset while a low P-value suggests that the two datasets have some sort of dependence. Elevation had the lowest P-value of 4.01×10^{-11} of all the parameters. The highest R^2-value occurs for whole basin relief at 0.44. R^2-values are most likely low because of the small number of data points, but can still be used to compare with the others in the same data set.

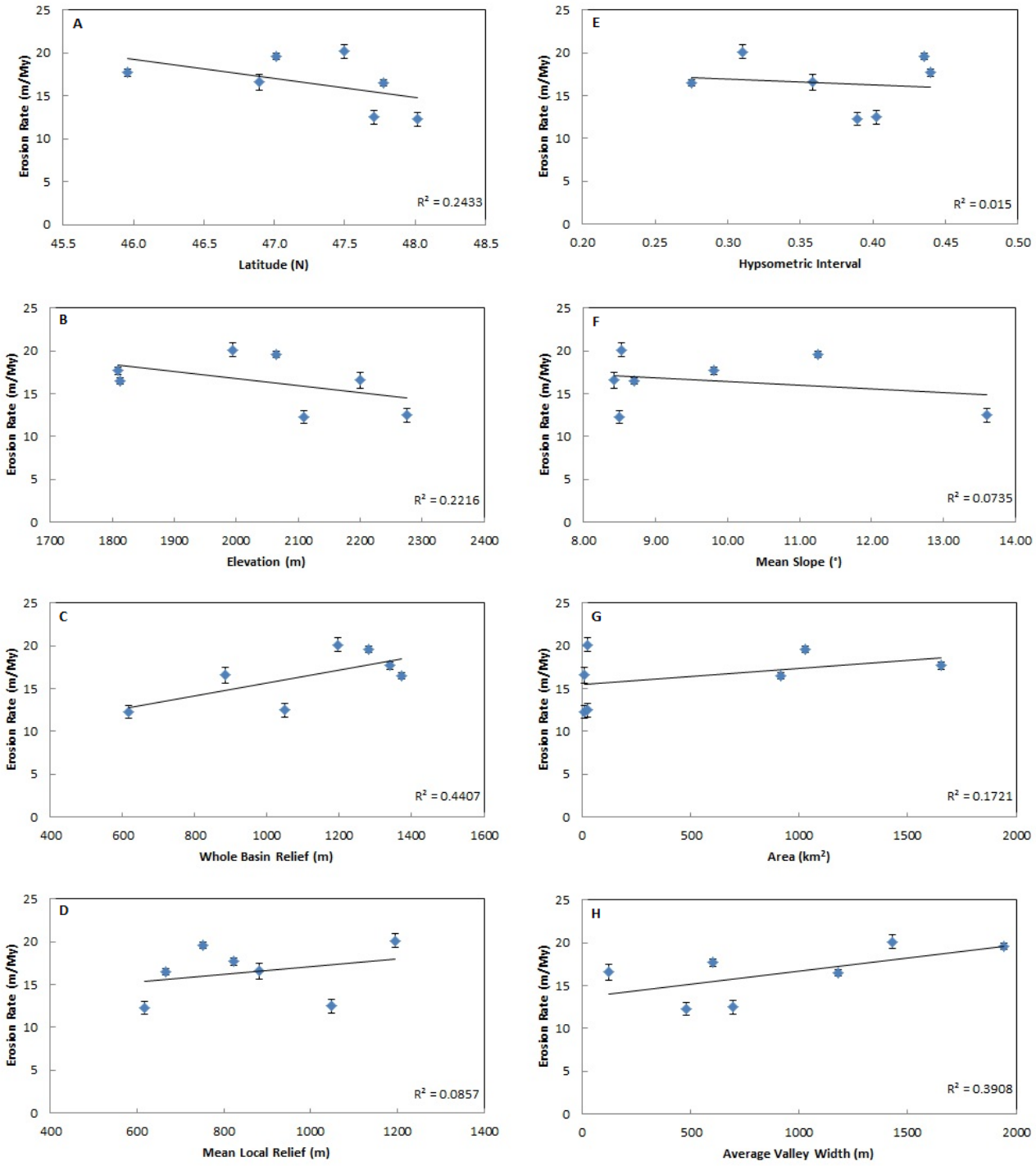

Figure 10. Erosion rates compared to latitude (A), elevation (B), whole basin relief (C), mean local relief (D), hypsometric interval (E), mean slope (F), basin area (G), and average valley width (H). Black line is the linear regression.

Table 4. P-values and R^2-values for erosion rate versus all basin parameters. Minimum values are shown in light grey and maximum values are shown in dark grey.

	Latitude	Elevation	Whole Basin Relief	Mean Local Relief	Hypsometric Interval	Mean Slope	Area	Average Valley Width
P-value	7.27519E-08	4.00845E-11	4.48833E-05	3.90219E-05	9.38277E-06	7.34E-04	8.60E-02	8.77E-03
R^2-value	0.2433	0.2216	0.4407	0.0857	0.015	0.0735	0.1721	0.3908

CHAPTER 5

DISCUSSION

Basin Parameters

Linear regressions comparing basin averaged erosion rates to both latitude and elevation show that erosion rates trend negatively and explain around twenty percent of the variance in both cases (Figure 10A and 10B). At higher latitudes and elevations, temperatures decrease which lowers chemical weathering but enhances mechanical weathering by frost cracking (Hales and Roering, 2009). Although frost cracking and other periglacial processes may produce more sediment in these colder environments, the rate of erosion is controlled by the ability to transport this sediment down the hillslopes to the streams. The diffusive-like hillslope sediment transport mechanisms observed throughout the Hangay Mountains result in very slow rates of transport. The fact that no recent or old mass wasting events were observed during the 2-week field excursion is further evidence to suggest that erosion rates are limited by both the rate of production and hillslope transport mechanisms, which are believed to be dominated by creep-based periglacial processes.

Figure 10C and 10D show comparisons of erosion rates with the amount of relief in the basin. Part C shows the whole basin relief, while part D shows the mean local relief. The mean local relief was found in basins with an area greater than 50 km^2 by averaging the relief found in each of the tributary drainage areas. Because of large floodplain areas in the bigger basins, the mean local relief estimate is lower for these large basins and does not take into account lower elevation areas near the sampling location. Therefore, the whole basin relief parameter is more illustrative of the basin-average erosion rates ($R^2 = 0.44$). In fact, it has the highest R^2-value of all the basin parameter comparisons. Erosion rate versus relief is compared to published results in the two following sub-sections.

Hypsometric interval and mean slope are not good indicators of the erosion rates found in the Hangay Mountains as shown by Figure 10E and 10F, with the two lowest R^2-values of the comparisons. The large range in area of the basins sampled (~6 km^2 to over 1600 km^2) probably accounts for the determination of the highest P-value. This suggests that the correlation found by the linear regression is most likely accredited to random chance.

A positive relationship was found between average valley floor width for 5 km upbasin from the sample site and basin-average erosion rate, as shown by Figure 10H. Therefore, a wider floodplain is tied to higher erosion rates. At first, this seems counter-intuitive because one might assume the storage of sediment in the floodplain would reduce overall basin-average erosion rates (Dunai, 2010). But, the fact that larger floodplains are produced by larger streams probably accounts for the stream's ability to move more sediment in general.

With the addition of eighteen samples still waiting analysis at Purdue University's PRIME lab, the statistics of these comparisons will become more accurate and the story they tell could emerge with greater reliability.

Data Comparisons

Ahnert (1970)

In a pioneering study, Frank Ahnert compared erosion rates of twenty large, mid-latitude, temperate river basins to their mean local relief (1970). He concluded that basin averaged erosion rates are linearly proportional to mean local relief. He proposed that to reduce the relief of a landscape to ten percent of its original relief would take 11 My. Including the influence of isostatic compensation, it would take a minimum of 18.5 My.

In comparing our results with those from Ahnert (1970), it is easy to see that for the amount of relief in the Hangay, our erosion rates are much lower than expected (Figure 11). This could be caused by many reasons including the fact that the latitude of our study area is higher than that of most of Ahnert's samples, therefore factors such as permafrost play a role in altering the erosion rates. Also, in our study area, there is no evidence of mass wasting. Landslides and rock avalanches would speed erosion by moving large masses of material very quickly, but a landscape such as that found in the Hangay is dominated by slower diffusional sediment transport. Although the relationship is not yet clear, floodplain storage could also lower the erosion rates measured by cosmogenic nuclides in the sediment. The potentially most important difference between our data and that of the Ahnert (1970) study is that because of both large valley floor widths and diffusional hillslope sediment transport, the erosion is transport limited. With few exceptions, the streams in the Hangay are not incising into fresh bedrock, but merely flowing on top of previously deposited alluvium. If fresh bedrock is not being introduced to the channel from the hillslope mass wasting events, and the channels themselves are not eroding into bedrock, the overall erosion rate is likely limited to the rate at which sediment can be produced and transported from hillslopes, rather than by the rate at which rivers are incising or the strength of the bedrock (e.g., Montgomery and Brandon, 2002).

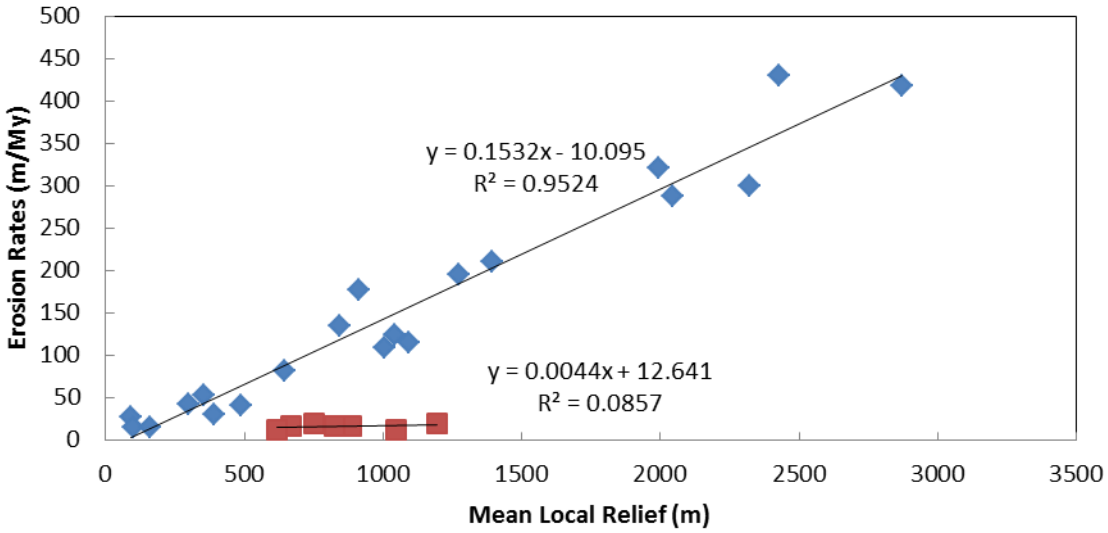

Figure 11. Erosion rates versus mean local relief comparing data from this study with the dataset of Ahnert (1970). The Ahnert data is shown in blue diamonds, while ours is shown as red squares.

Portenga and Bierman (2011)

Portenga and Bierman (2011) compiled a data repository of many ^{10}Be outcrop and basin-averaged erosion rates and corresponding basin metrics from around the world. Because of the extreme variety in the distribution of samples, we only used basin samples from non-seismic areas indicated by a seismicity of less than 2 to compare to our data. Since their data set did not include mean local relief, we compared our erosion rates to theirs using whole basin relief (Figure 12). The Portenga and Bierman data set reports erosion rates from less than 1 m/My in Australia to over 4000 m/My in California and whole basin relief ranging from less than 200 m in areas such as Pennsylvania and Germany up to 7000 m in Bolivia and China. All of our basin-averaged erosion rates fall below a linear regression line fit through the Portenga and Bierman data.

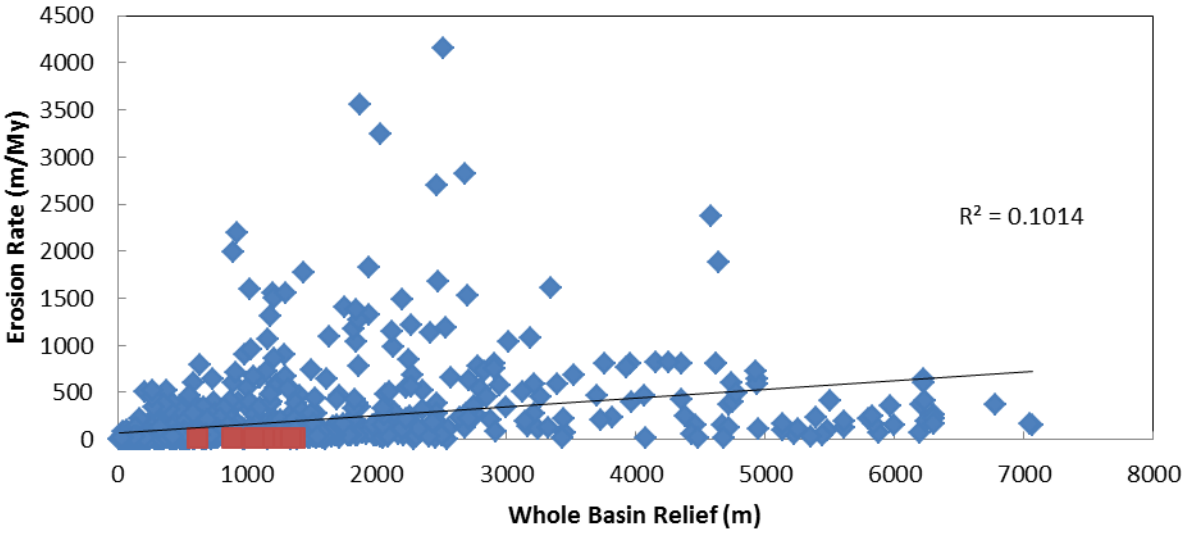

Figure 13. Basin-averaged erosion rate versus whole basin relief. Non-seismic basin data of Portenga and Beirman (2012) is shown as blue diamonds, while ours is shown as red squares.

Filtered by Climatic Region

One way to better relate the Hangay data to other basin-scale erosion data is to filter these data collections to only those closely matched by the climate (and by inference, the principal geomorphic processes responsible for the erosion and transport of sediment) of the Hangay Mountains. The Portenga and Bierman data were searched for samples from regions deemed "arid: cold steppe", "cold: dry winter with warm summer", and "polar: tundra." This allows effects from permafrost to be present in a majority of the comparison basins as well as more similarity between yearly mean temperature and average rainfall between this study and comparative sample locations.

When the climate-filtered data is compared to our data, substantial scatter remains. Some of the Portenga and Bierman data that has higher erosion rates have been excluded by this filter, but many with an erosion rate well over 1000 m/My are still present (Figure 13). The highest relief is near 7000 m for a sample in China; about the same as before.

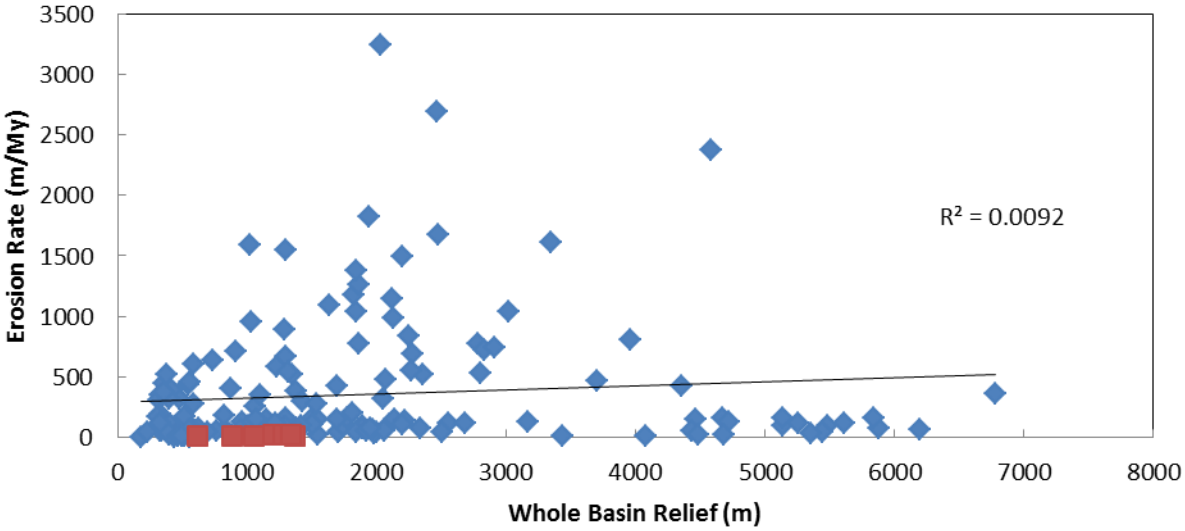

Figure 13. Basin-averaged erosion rate versus whole basin relief. The Portenga and Beirman (2011) data set is filtered by similar climatic regions (blue diamonds) in comparison to the data from the Hangay Mountains (red squares).

Filtered by Geomorphic Setting

More informed comparisons can also be made if the Portenga and Bierman (2011) compilation is categorized by geomorphic settings. For this filter, the Portenga and Bierman data set was reduced to basin-averaged erosion rates determined from "plateau" or "uplift" regions. By filtering by geomorphic setting, the trend now explains over forty percent of the variance in the data (Figure 14). Although still many times higher than ours, all but two of the erosion rates now fall below 1000 m/My implying that plateau and uplift regions have lower erosion rates overall than found in the entire non-seismic data set.

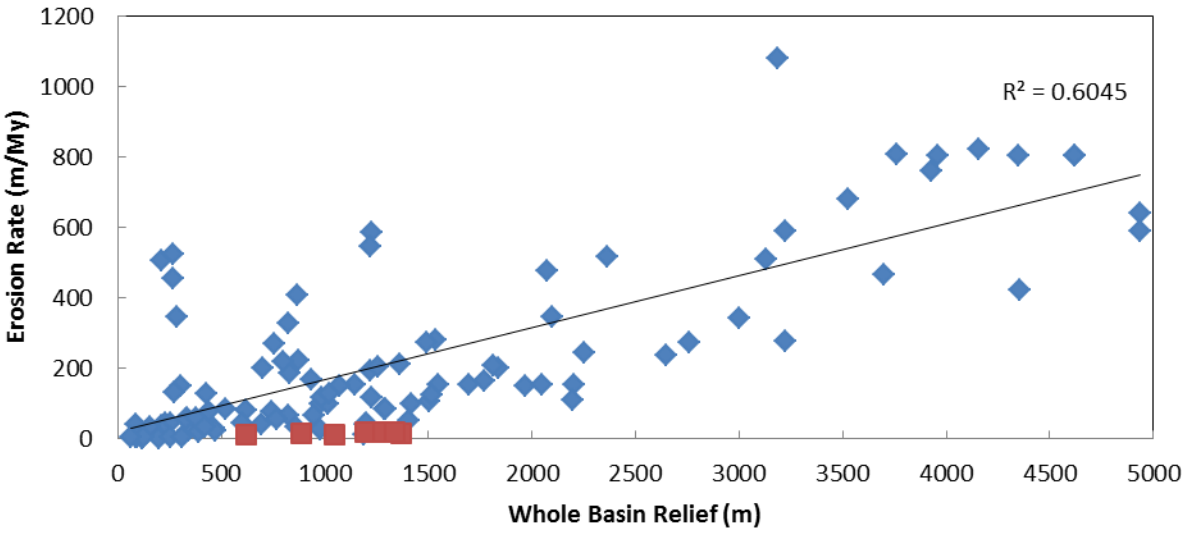

Figure 14. Basin-averaged erosion rate versus whole basin relief. The Portenga and Beirman (2011, blue diamonds) data was filtered to include only plateau and uplift settings, somewhat analogous to the Hangay Mountains (red squares).

Filtered by Climatic Region and Geomorphic Setting

In the next step, we combined the climate and geomorphic setting data into a single compilation of available global basin-average erosion rate data similar in these two parameters to the Hangay Mountains (Figure 15). The trend explains more than fifty-three percent of the variance in the Portenga and Bierman data set. The data from the Hangay lie below erosion rates predicted from this analysis, similar to what was shown in the Ahnert comparison (Figure 11). Because of the climate and geomorphic setting filter analysis, we can confidently state that the explanation of those regional differences now falls short. Instead, the differences in erosion rates are likely due to the fact that the streams in the Hangay are eroding into alluvium as opposed to bedrock, and are located in a dominantly diffusional landscape. The erosion is limited to the amount of sediment that can be transported by the streams.

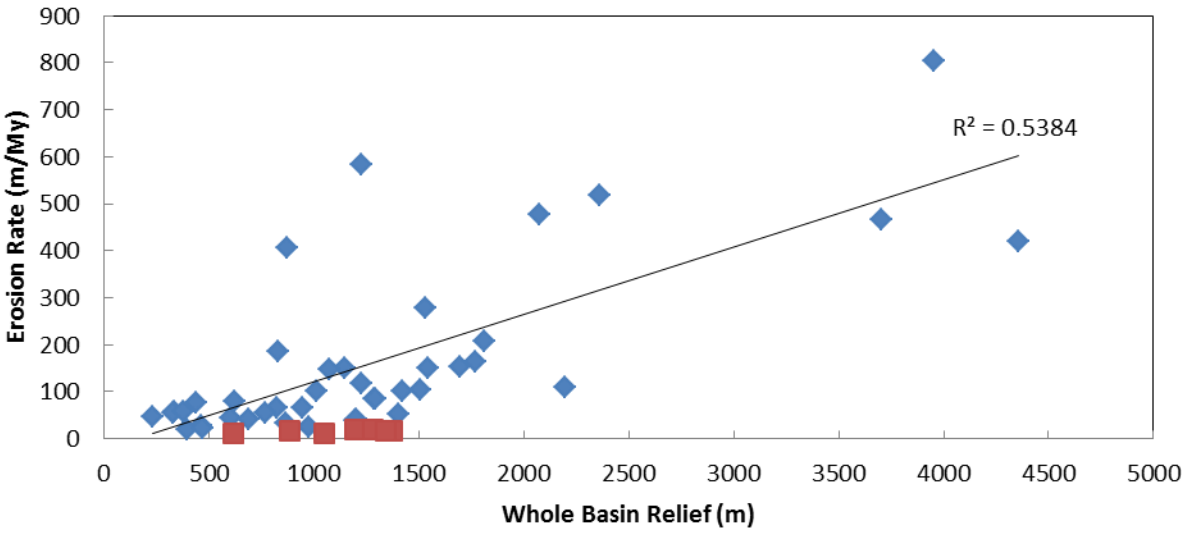

Figure 15. Basin averaged erosion rates versus whole basin relief. The Portenga and Beirman (2011; blue diamonds) data was filtered to include climatic and geomorphic settings similar to the Hangay Mountains (red squares).

Matmon et al. (2009)

Matmon et al. (2009) well illustrated differences in erosion rates from varying settings around the world (Figure 16). The figure shows erosion rates spanning eight orders of magnitude from very low rates found from desert pavements to extremely fast rates in the quickly uplifting Himalaya. With erosion rates ranging from roughly 12 m/My to 20 m/My, the drainage basin-average erosion rates from the Hangay Mountains are of the same magnitude as basin-averaged erosion rates observed in the tectonically inactive regions, such as the southern Appalachians, Sri Lanka, and Namibia.

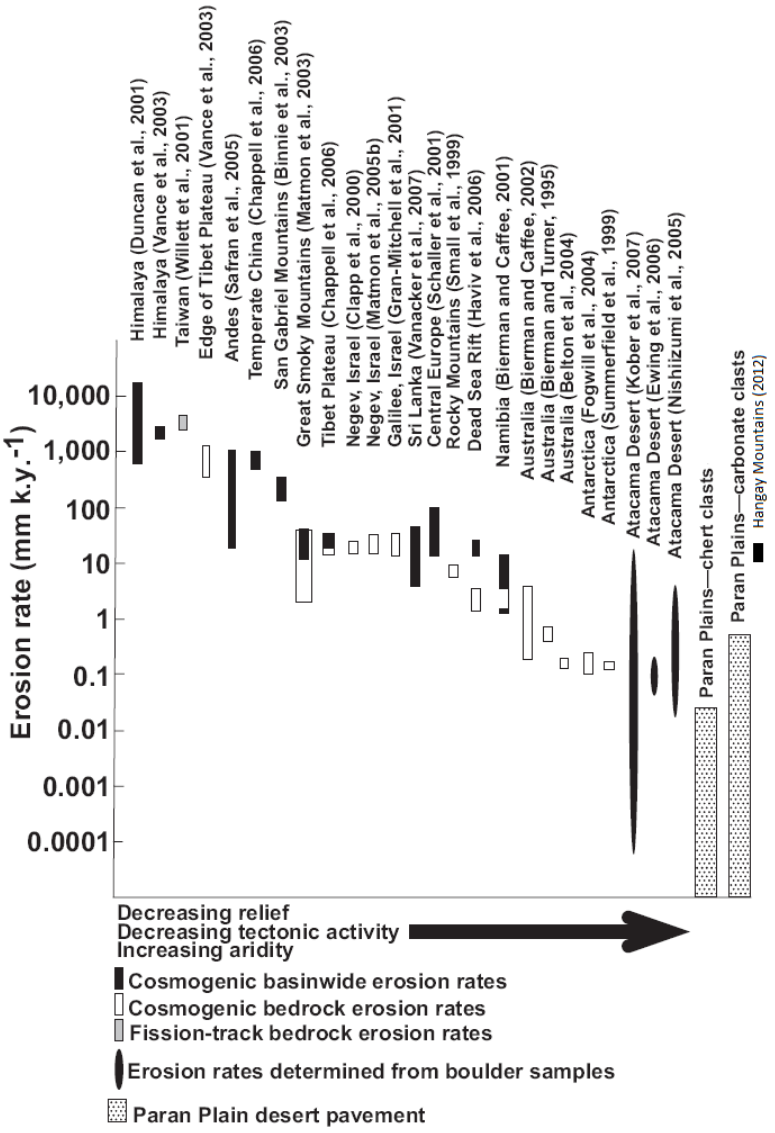

Figure 16. Erosion rates observed in different environments around the world. Modified from Matmon et al. (2009). Erosion rates from the Hangay are of a similar magnitude to those from the Great Smoky Mountains, Sri Lanka, and Namibia.

Landman (2007)

Rachel Landman studied apatite grains in four granite samples from the Hangay Mountains to determine their (U-Th)/He cooling ages (Landman, 2007). These ages represent when the granites passed through their closure temperature of around 70°C (Dunai, 2005). Landman's four samples came from an area near the crest of the Hangay Mountains within the same study area as the cosmogenic samples in this paper. The

cooling ages ranged from about 100 to 110 million years ago with a mean of almost 108 My. Assuming a geothermal gradient of between 25°C to 30°C, the 70°C closure temperature would occur at a depth of 2.3 km to 2.8 km below the surface. If the apatite grains in the granite passed through this closure temperature isotherm around 108 million years ago, a long-term rate of exhumation could be calculated to be between 21 m/My to 26 m/My. These rates of exhumation are interestingly close to the 12 m/My to 20 m/My found in this study.

Data from Landman's work doesn't explain the speed at which these granites reached the surface; more work finding exhumation profiles is needed to determine that. They could have exhumed rapidly and have been at the surface for a very long time. The granites could have risen slowly and then sped up to reach the surface only recently. But, if we assume these granites exhumed slowly and steadily since about 100 My, it is possible that the Hangay Mountains in Mongolia have been slowly eroding at a rate of around 20 m/My for at over 100 million years.

CHAPTER 6

CONCLUSIONS

Beryllium-10 derived basin-average erosion rates were found to be between 12 m/My and 20 m/My for seven basins in the eastern Hangay Mountains of Mongolia. These were determined using a production rate of 5.12 atoms g^{-1} yr^{-1} (Lal, 1991). The basin-average erosion rates are of the same magnitude as basin-average erosion rates observed in tectonically inactive regions, such as the southern Appalachians, Sri Lanka, and Namibia.

Comparing basin-average erosion rates to basin parameters, whole basin relief had the highest calculated R^2-value of 0.44. Erosion rate and elevation had the lowest P-value of 4.01×10^{-11}. No strong relationships were seen between erosion rate and mean slope angle, hypsometric integral, area, or mean local relief.

The basin-average erosion rates observed in the Hangay were compared to Ahnert's 1970 study in which he found a linear relationship between erosion rate and mean basin relief. For the amount of relief in the Hangay, our erosion rates are much lower than Ahnert's relationship would predict. The data compilation by Portenga and Bierman (2011) was reduced to samples with only the same climatic and geomorphic settings as found in the Hangay to minimize regional differences. The data from the Hangay still lie much lower than expected from this analysis.

The differences in erosion rates from the Hangay Mountains compared to other places around the world are likely due to the fact that the streams in the Hangay are eroding into alluvium as opposed to bedrock, and are located in a dominantly diffusional landscape with no observed evidence of recent or old mass wasting events. The erosion is limited to the amount of sediment that can be transported by the streams.

Nine more basin-average samples and seven ridgetop samples await AMS analysis at Purdue University's PRIME laboratory. With the addition of these samples, the statistical relationships between basin-average erosion rate and basin parameters may become more pronounced.

Also, taking samples to determine both ridgetop and basin wide erosion rates allows the comparison of the two to see how and if the relief of the area is changing. Three possibilities could be found:

(1) If ridge line erosion rates are greater than basin wide erosion rates, relief of the area would be decreasing.

(2) If the ridge line erosion rates are less than the basin wide erosion rates, relief would be increasing.

(3) Ridge top and basin wide erosion rates could be nearly the same, implying that relief of the area is in quasi-steady state, for at least the timescale represented by ^{10}Be geochronology.

If the results of the basin-average erosion rate and ridgetop erosion rate samples tend toward the third option, the landscape would be evolving in the manner described by Hack's (1960) principle of dynamic equilibrium. The change in relief or lack thereof can be used in conjunction with other ongoing studies with seismology, thermochronology, fish genetics, and geochemistry, to decipher the rate, timing, and dynamic lithosphere and asthenospheric processes responsible for the uplift of the Hangay Mountains.

APPENDIX A

LABORATORY PROCEDURES

*Note: The Al carrier in step 4 and all of step 6 are not used for single nuclide analysis.

Location: **Sample:** **Date:**

1 Sieved rock 250-500µm

2 HCl leach — 6N HCl + 0.03% H_2O_2; 10ml/g; 12 hours sub-boiling

3 HF leach — 1%HF + 1% HNO_3

	HF	HNO_3	H_2O	Canister x amount	Initial	Final
1. 7.5g/L; 9 hours at 90°C						
2. 15g/L; 9 hours at 90°C						
3. 15g/L; 9 hours at 90°C						

4 Be + Al Carrier — Teflon beaker + quartz + Be carrier (0.3g) + Al carrier (2g)

quartz (g)		
Be carrier (g)	concentration	name
Al carrier (g)	concentration	name

5 HF + HNO_3 — HF (5ml/g) + HNO_3 (0.3ml/g)

HF (ml)	HNO_3 (ml)

lid on beaker; heat 1-2hrs until completely dissolved; cool down; transfer to tared bottle

6 Al aliquot — weigh solution + take aliquot

solution (g)	aliquot (g)

dry down completely

7 $HClO_4$ fuming

1. 10mL H_2O + 10mL HNO_3 + 4mL $HClO_4$
2. H2O rinse + 2mL HClO4
3. H_2O rinse + 2mL $HClO_4$

dry down completely between fuming steps

dry (ready for columns)

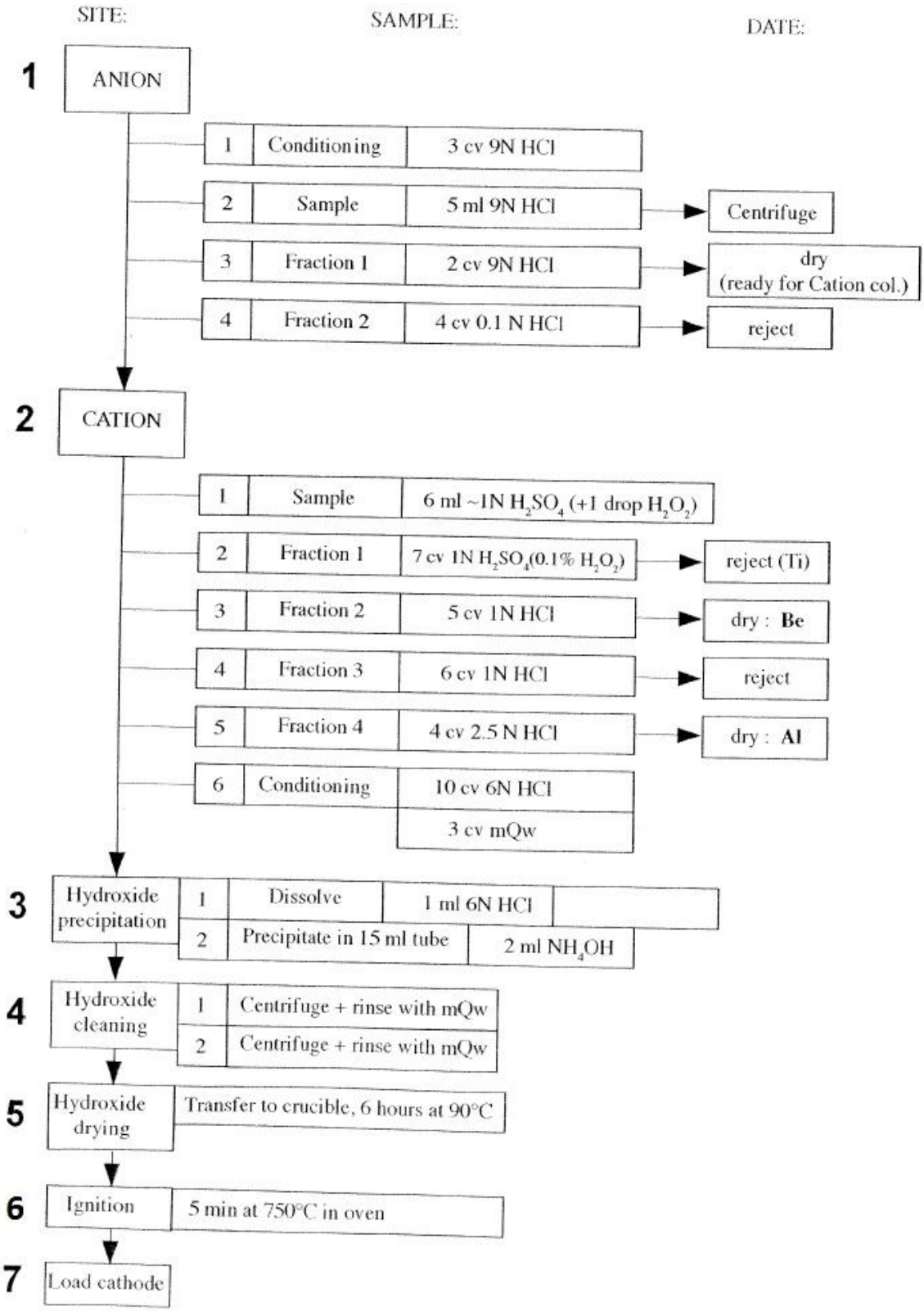
SITE:
SAMPLE:
DATE:
1
ANION
1 Conditioning 3 cv 9N HCl
2 Sample 5 ml 9N HCl
Centrifuge
3 Fraction 1 2 cv 9N HCl
dry (ready for Cation col.)
4 Fraction 2 4 cv 0.1 N HCl
reject
2
CATION
1 Sample 6 ml ~1N H_2SO_4 (+1 drop H_2O_2)
2 Fraction 1 7 cv 1N H_2SO_4(0.1% H_2O_2)
reject (Ti)
3 Fraction 2 5 cv 1N HCl
dry : Be
4 Fraction 3 6 cv 1N HCl
reject
5 Fraction 4 4 cv 2.5 N HCl
dry : Al
6 Conditioning 10 cv 6N HCl
3 cv mQw
3
Hydroxide precipitation
1 Dissolve 1 ml 6N HCl
2 Precipitate in 15 ml tube 2 ml NH_4OH
4
Hydroxide cleaning
1 Centrifuge + rinse with mQw
2 Centrifuge + rinse with mQw
5
Hydroxide drying
Transfer to crucible, 6 hours at 90°C
6
Ignition
5 min at 750°C in oven
7
Load cathode

REFERENCES

Ahnert, F., 1970. Functional relationships between dunudation, relief, and uplift in large mid-latitude drainage basins: American Journal of Science, v. 268, p. 243-263.

Anderson, R.S., Repka, J.L., and Dick, G.S., 1996. Explicit treatment of inheritance in dating depositional surfaces using in situ 10Be and 26Al: Geology, v. 24, no.1, p. 47-51.

Balco, G. 2001. Cosmogenic isotope production rates over large areas: http://depts.washington.edu/cosmolab/P_by_GIS.html.

Balco, G. 2006. Converting Al and Be isotope ratio measurements to nuclide concentrations in quartz. http://hess.ess.washington.edu/math/docs/common/ams_data_reduction.pdf.

Balco, G., Stone, J.O., Lifton, N.A., and Dunai, T.J., 2008. A complete and easily accessible means of calculating surface exposure ages or erosion rates from 10Be and 26Al measurements: Quaternary Geochronology, v. 3, p. 174—195.

Belmont, P., Pazzaglia, F.J., and Gosse, J.C., 2007. Cosmogenic 10Be as a tracer for hillslope and channel sediment dynamics in the Clearwater River, western Washington State: Earth and Planetary Science Letters v. 264, p. 123-125.

Bierman, P.R. and E. J. Steig, 1996. Estimating rates of denudation using cosmogenic isotope abundances in sediment, Earth Surface Processes and Landforms, v. 21, p. 125-139.

Bierman, P.R., Caffee, M.W., Davis, P.T., Marsella, K., Pavich, M., Colgan, P., Mickelson, D., and Larsen, J., 2002. Rates and timing of earth surface processes from in-situ-produced cosmogenic Be-10: Reviews in Mineralogy and Geochemistry, v. 50, no.1, p. 145-205.

Brozovic, N., Burbank, D.W., and Meigs, A.J., 1997. Climatic Limits on Landscape Development in the Northwestern Himalaya: Science, v. 276, p. 571-574.

Burbank, D.W., Leland, J., Fielding, E., Anderson, R.S., Brozovic, N., Reid, M.R., and Duncan, C., 1996. Bedrock incision, rock uplift and threshold hillslopes in the northwestern Himalayas: Nature, v. 379, p.505-510.

Burbank, D.W. and Anderson, R.S., 2012. Tectonic Geomorphology, 2nd edition: Blackwell Publishing Ltd.

Cunningham, W.D., 2001. Cenozoic normal faulting and regional doming in the southern Hangay region, Central Mongolia: implications for the origin of the Baikal rift province: Tectonophysics, v. 331, p. 389-411.

Cyr, A.J. and Granger, D.E., 2008. Dynamic equilibrium among erosion, river incision, and coastal uplift in the northern and central Apennines, Italy: Geology, v. 36, no. 2, p. 103-106.

Cyr, A.J., Granger, D.E., Olivetti, V., and Molin, P., 2010. Quanitfying rock uplift rates using channel steepness and cosmogenic nuclide-determined erosion rates: Examples from northern and southern Italy: Lithosphere, v. 2, no. 3, p. 188-198.

Davis, W.M., 1889. The Rivers and valleys of Pennsylvania: National Geographic Magazine, v. 1, no. 3, p. 183-253.

Davis, W.M., 1899. The geographic cycle: Geography Journal, v. 14, p. 481-504.

Desilets, D., and M. Zreda, 2003. Spatial and temporal distribution of secondary cosmic-ray nucleon intensities and applications to in situ cosmogenic dating: Earth and Planetary Science Letters, 206, p. 21-42.

Desilets, D., M. Zreda, and T. Prabu, 2006. Extended scaling factors for in situ cosmogenic nuclides: New measurements at low latitude: Earth and Planetary Science Letters, 246, p. 265-276.

Devyatkin, E.V., 1975. Neotectonic structures of western Mongolia (in Russian). In:Mesozoic and Cenozoic Tectonics and Magmatism of Mongolia: Nauka, Moscow, p. 264-282.

Dunai, T.J., 2000. Scaling factors for production rates of in situ produced cosmogenic nuclides: a critical reevaluation: Earth and Planetary Science Letters, 176, p. 157-169.

Dunai, T.J., 2005. Forward modeling and interpretation of (u/Th)/He ages. In: Reiners, P.W., Ehlers, T.A., (eds.) Low-Temperature Thermochronology: Techniques, Interpretations, and Applications: Reviews in Mineralogy and Geochemistry, v. 58, p. 259-274.

Dunai, T.J., 2010. Cosmogenic Nuclides: Principles, Concepts, and Applications in the Earth Surface Sciences: Cambridge University Press, UK.

Egholm, D.L., Nielson, S.B., Pedersen, V.K., and Lesemann, J.E., 2009. Glacial effects limiting mountain height: Nature, v. 460, p. 884-888.

Finkel, R.C., Owen, L.A., Barnard, P.L., and Caffee, M.W., 2003. Beryllium-10 dating of Mount Evert moraines indicates a strong monsoon influence and glacial synchroneity throughout the Himalaya: Geology, v. 31, no. 6, p. 561-564.

Frankel, K. L., Wegmann, K. W., Bayasgalan, A., Carson, R. J., Bader, N. E., Adiya, T., Bolor, E., Durfey, C. C., Otgonkhuu, J., Sprajcar, J., Sweeney, K. E., Walker, R. T., Marstellar, T. L., and Gregory, L., 2010. Late Pleistocene slip rate of the Höh Serh–Tsagaan Salaa fault system, Mongolian Altai and intracontinental deformation in central Asia: Geophysical Journal International, v. 183, no. 3, p. 1134-1150; DOI: 1110.1111/j.1365-1246X.2010.04826.x.

Fuller, T.K., Perg, L.A., Willenbring, J.K., and Lepper K., 2009. Field evidence for climate-driven changes in sediment supply leading to starth terrace formation: Geology, v. 37, no. 5, p. 467-470.

Gilbert, G.K., 1909. The convexity of hilltops: Journal of Geology, v. 17, p. 344-350.

Gosse, J., and Philips, F., 2001. Terrestrial in situ cosmogenic nuclides: theory and application: Quaternary Science Reviews, v. 20, p. 1475-1560.

Gosse, J, 2009. Applications of Terrestrial In situ Consmogenic Nuclides, CANQUA Short Course – Simon Fraser University. Dalhousie University.

Granger, D.E., Kirchner, J.W., and Finkel, R., 1996. Spatially averaged long-term erosion rates measured from in-situ produced cosmogenic nuclides in alluvial sediment: Journal of Geology, v. 104, p. 249-257.

Hack, J.T., 1960. Interpretation of erosional topography in humid temperate regions: American Journal of Scice, v. 258A, p. 80-97.

Hales, T. C. & J. J. Roering, 2009: A frost "buzzsaw" mechanism for erosion of the eastern Southern Alps, New Zealand. Geomorphology, 107, 241-253 ff.

Hancock, G.S., Anderson, R.S., Chadwick, O.A., and Finkel, R.C., 1998. Dating fluvial terraces with 10Be and 26Al profiles: application to the Wind River, Wyoming: Geomorphology, v. 27, p. 41-60.

Hancock, G., and Kirwan, M., 2007. Summit erosion rates deduced from 10Be: Implications for relief production in the central Appalachians: Geology, v. 35, no. 1, p. 89-92.

Jolivet, M., Ritz, J., Vassallo, R., Larroque, C., Braucher, R., Todbileg, M., Chauvet, A., Sue, C., Arnaud, N., De Vicente, R., Arzhanikova, A., and Arzhanikova, S., 2007. Mongolian summits: An uplifted, flat, old but still preserved erosion surface: Geology, v. 35, no.10, p. 871-874.

Kooi, H. and Beaumont, C., 1996. Large0scale geomorphology classical concepts reconciled and integrated with contemporary ideas via a surface processes model: Journal of Geophysical Research, B, Solid Earth and Planets, v. 101(2), p. 3361-3386.

Lal, D., 1991, Cosmic-ray labeling of erosion surfaces: In situ nuclide production-rates and erosion models: Earth and Planetary Science Letters, v. 104, p. 424-439.Matmon, A., Bierman, P.R., Larsen, J., Southworth, S., Pavich, M., and Caffee, M., 2003. Temporally and spatially uniform rates of erosion in the southern Appalachian Great Smoky Mountains: Geology, v. 31, no. 2, p. 155-158.

Landman, R.L., 2007. Petrologic constraints on the sources of granites from the Hangay Mountains, central Mongolia: Dept. of Geology, Amherst College.

Lehmkuhl, F.; M. Klinge & G. Stauch, 2004: The extent of Late Pleistocene glaciations in the Altai and Khangai Mountains, 243-254ff in Ehlers J. and Gibbard, P. L. (ed.), Quaternary Glaciations - Extent and Chronology, Part III. Amsterdam.

Lifton, N.A., Bieber, J.W., Clem, J.M., Duldig, M.L, Evenson, P., Humble, J.E., and Pyle, R., 2005. Addressing solar modulation and long-term uncertainties in scaling in situ cosmogenic nuclide production rates: Earth and Planetary Science Letters, v. 239, p. 140-161.

Matmon, A., Bierman, P.R., Larsen, J., Southworth, S., Ravich, M., and Caffee, M., 2003. Temporally and spatially uniform rates of erosion in the southern Appalachian Great Smoky Mountains: Geology, v. 31, no. 2, p. 155-158.

Matmon, A., Simhai, O., Amit, R., Porat, N., McDonald, E., Benedetti, L., and Finkel, R., 2009. Desert pavement-coated surfaces in extreme deserts present the longest-lived landforms on Earth: GSA Bulletin, v. 121, no. 5-6, p. 688-697.

Montgomery, D.R., and Brandon, M.T., 2002, Topographic controls on erosion rates in tectonically active mountain ranges: Earth and Planetary Science Letters, v. 201, no. 3-4, p. 481-489.

Niemi, N.A., Oskin, M., Burbank, D.W., Heimsath, A.M., and Gabet, E.J., 2005. Effects of bedrock landslides on cosmogenically determined erosion rates, v. 237, p. 480-498.

Pazzaglia, F.J., 2003. Landscape evolution models: Development in Quaternary Science, v. 1, p. 247-273.

Penck, W., 1953. Morphological analysis of landforms: New York, St. Martin's Press, p.429.

Portenga, E., and Bierman, P.R., 2011. Understanding earth's eroding surface with 10Be: GSA Today.

Powell, J.W., 1875. Exploration of the Colorado River of the West: Washington, D.C., U.S. Government Printing Office, 291 pages.

Refsnider, K.A., 2010. Dramatic increase in late Cenozoic alpine rates recorded by cave sediment in the southern Rocky Mountains: Earth and Planetary Science Letters, v. 297, p. 505-511.

Small, E.E., Anderson, R.S., Repka, J.L., and Finkel, R., 1997. Erosion rates of alpine bedrock summit surfaces deduced from in-situ 10Be and 26Al: Earth and Planetary Science Letters, v. 150, p. 413-425.

Stock, G.M., Frankel, K.L., Ehlers T.A., Schaller, M., Briggs, S.M., and Finkel, R.C., 2009. Spatial and temporal variations in denudation of the Wasatch Mountains, Utah, USA: Lithosphere, v. 1, no. 1, p. 34-40.

Stone, J.O., 1999. A consistent Be-10 production rate in quartz – muons and altitude scaling: AMS-8 Proceedings Abstract Volume, Vienna, Austria.

Stone, J. O., 2000, Air pressure and cosmogenic isotope production: Journal of Geophysical Research, v. 105, no. B10, p. 23,753-723,759.

Vassallo, R., Jolivet, M., Ritz, J.F., Braucher, R., Larroque, C., Sue, C., Todbileg, M., and Javkhlanbold, D., 2007. Uplift age and rates of the Gurvan Bogd system (Gobi-Altay) by apatite fission track analysis: Earth and Planetary Science Letters, v. 259, no. 3-4, p. 333-346.

Vassallo, R., Ritz, J., and Carretier, S., 2011. Control of geomorphic processes on 10Be concentrations in individual clasts: Complexity of the exposure history in Gobi-Altay range (Mongolia): Geomorphology, v. 135, p. 35-47.

Vermeesch, P., 2007, CosmoCalc: an Excel add-in for cosmogenic nuclide calculations: Geochemistry, Geophysics, and Geosystems (in press).

Von Blackenburg, F., 2005. The control mechanisms of erosion and weathering at basin scale from cosmogenic nuclides in river sediment: Earth and Planetary Science Letters, v. 237, p. 462-479.

Walker, M., 2005. Quaternary Dating Methods: John Wiley & Sons Ltd.

Walker, R. T., Nissen, E., Molor, E., and Bayasgalan, A., 2007. Reinterpretation of the active faulting in central Mongolia. Geology, v. 35**,** p. 759-762.

Yanites, B.J., Tucker, G.E., and Anderson, R.S., 2009. Numerical and analytical models of cosmogenic radionuclide dynamics in landslide-dominated drainage basins, v. 114, doi:10.1029/2008JF001088.